



## Corrosion behavior of GeO<sub>2</sub> and Sc<sub>2</sub>O<sub>3</sub> Coatings on AZ31 Alloy

L. SUTHA<sup>1,2</sup> and A. CYRIL<sup>2\*</sup>

<sup>1,2</sup>Department of Industrial Chemistry, Alagappa University, Karaikudi, India.

<sup>2</sup>Department of Chemistry, Raja Doraisingam Government Arts College, Sivaganga, Tamilnadu, India.

\*Corresponding author E-mail: cyrilchemistry@gmail.com

<http://dx.doi.org/10.13005/ojc/370224>

(Received: March 18, 2021; Accepted: April 21, 2021)

### ABSTRACT

In this work, GeO<sub>2</sub> (germanium dioxide) and Sc<sub>2</sub>O<sub>3</sub> (scandium trioxide) were developed as coatings on AZ31 alloy using polymer binder. The coatings were characterized using X-ray crystallography procedure (XRD), infrared spectrum of absorption or emission of a solid procedure (FTIR), Raman spectroscopy procedure, surface examination by FESEM. The corrosion studies were analyzed using a three electrode system in 3.5% NaCl electrolyte. The bare AZ31 alloy showed open circuit potential ( $E_{corr}$ ) of -1.7 V (SCE) and the corrosion current density ( $i_{corr}$ ) of  $3.4 \times 10^{-4}$  mA/cm<sup>2</sup>, while the Sc<sub>2</sub>O<sub>3</sub> coated AZ31 alloy exhibited  $E_{corr}$  of -1.4 V (SCE) and the  $i_{corr}$  of  $5.4 \times 10^{-9}$  mA/cm<sup>2</sup> and while the GeO<sub>2</sub> coated AZ31 alloy exhibited  $E_{corr}$  of -1.3 V (SCE) and the  $i_{corr}$  of  $2.59 \times 10^{-9}$  mA/cm<sup>2</sup>. The results reveal that the GeO<sub>2</sub> coated AZ31 alloy demonstrated higher corrosion resistance than of bare AZ31 alloy and Sc<sub>2</sub>O<sub>3</sub> coated AZ31 alloy.

**Keywords:** Mg alloys, AZ31, GeO<sub>2</sub>, Sc<sub>2</sub>O<sub>3</sub>, Corrosion.

### INTRODUCTION

Magnesium alloys find many applications in space and aerospace applications due to high strength and low density. Even though, they suffer more corrosion due to the more negative electromotive force in the series<sup>1-4</sup>. Many attempts executed and reported to reduce the corrosion susceptibility of Mg alloys in aqueous medium applications<sup>5-12</sup>. Surface coatings demonstrated enhanced performance for magnesium alloys<sup>13-15</sup>. Recently, Wu *et al.*, fabricated diamond like DLC/AlN/Al coating on AZ31 using sputtering method and demonstrated a noble shift in the corrosion potential of AZ31 alloy in 3.5% NaCl solutions<sup>13</sup>. Graphene

based coatings were developed by Han *et al.*, by anodically oxidized and more noble shift around -1.15 V (SCE) in in 3.5% NaCl electrolyte<sup>14</sup>. WC coatings also developed by plasma electrolytic oxidation on AZ31 alloy and the author's demonstrated positive shift in corrosion potential<sup>15</sup>. However, there is much scope to improve the resistance against corrosion of Mg alloys for surface coatings by tuning the porosity and with suitable binders.

In this work, GeO<sub>2</sub> (germanium dioxide) and Sc<sub>2</sub>O<sub>3</sub> (scandium trioxide) were developed as coatings on AZ31 alloy using polymer binder. The bare AZ31 alloy showed open circuit potential ( $E_{corr}$ ) of -1.7 V (SCE) and the corrosion current density



( $i_{\text{corr}}$ ) of  $3.4 \times 10^{-4}$  mA/cm<sup>2</sup>, while the Sc<sub>2</sub>O<sub>3</sub> coated AZ31 alloy exhibited  $E_{\text{corr}}$  of -1.4 V (SCE) and the  $i_{\text{corr}}$  of  $5.4 \times 10^{-9}$  mA/cm<sup>2</sup> and while the GeO<sub>2</sub> coated AZ31 alloy exhibited  $E_{\text{corr}}$  of -1.3 V (SCE) and the  $i_{\text{corr}}$  of  $2.59 \times 10^{-9}$  mA/cm<sup>2</sup>. The results reveal that the GeO<sub>2</sub> coated AZ31 alloy demonstrated higher corrosion resistance than of bare AZ31 alloy and Sc<sub>2</sub>O<sub>3</sub> coated AZ31 alloy. The novelty of this work is on the fabrication of in-organic materials like oxides coatings formulation on the AZ31 alloy using organic binder, which showed effective role on the corrosion resistance enhancement of AZ31 alloy. The implications of this work may pave new pathways for Mg alloys corrosion resistance improvement.

## MATERIALS AND METHODS

### Chemicals

Germanium (IV) oxide (GeO<sub>2</sub>, 99.99%, CAS No: 1310-53-8) and Scandium(III) oxide (Sc<sub>2</sub>O<sub>3</sub>, 99.995%, CAS No: 12060-08-1), Poly(ethylene glycol) (PEG<sub>3</sub>, Bioultra 8000, CAS No: 25322-68-3), were purchased from Merck & Co.

### Sample preparation

The AZ31 alloy sheet was procured and cut into 11 x 11 x 5 mm dimension using wire EDM. Further, the samples were undergone metallurgical polishing before the application of coating on AZ31 alloy. Metallurgical polishing was employed using 200 to 1200 SiC grit polishing papers and finally treatment with 0.5 microns diamond paste cloth polishing. The samples were then washed to remove the polishing impurities and dried at room temperature.

### Electrode Preparation

The oxide powders of GeO<sub>2</sub> and Sc<sub>2</sub>O<sub>3</sub> were taken in 3 mg weight (respectively for each electrode) and added with 10 mL PEG-ethanol binder solution at 50°C and stirred for 4 h until homogeneous mixture formed. Then the mixed slurry was drop casted on AZ31 alloy and dried for 24 hours.

### Electrochemical experiments

Corrosion behavior of uncoated AZ31, Sc<sub>2</sub>O<sub>3</sub> and GeO<sub>2</sub> coatings over AZ31 alloy was studied in 3.5% NaCl medium with an assembly consisting of three electrode system, where Pt as counter electrode, AZ31 alloy samples with and without coatings were as working electrodes and SCE as reference electrode.

## RESULTS AND DISCUSSION

### XRD analysis

The phase purity and crystallinity of uncoated AZ31, Sc<sub>2</sub>O<sub>3</sub> coated AZ31 alloy and GeO<sub>2</sub> coated AZ31 alloy was characterized by XRD analysis and presented in Figures 1-3.

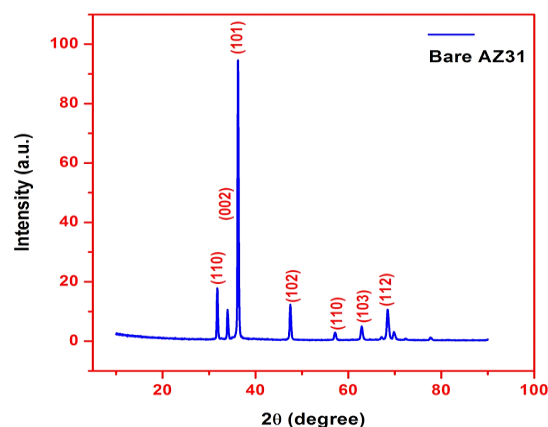
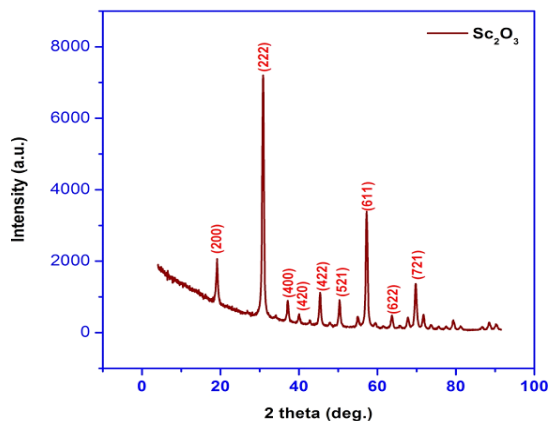
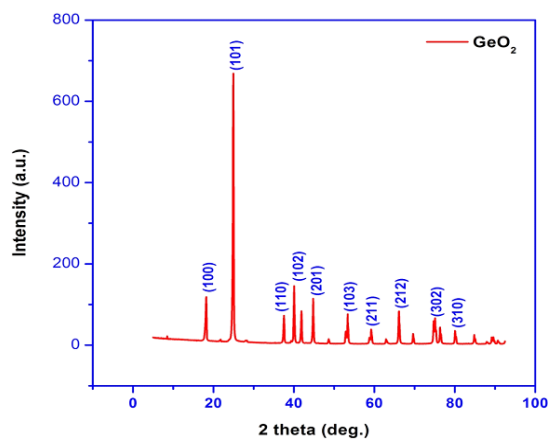


Fig. 1. X-ray diffraction pattern of AZ31 alloy

The pure AZ31 alloy X-ray diffraction peaks matched with the standard JCPDS file no 35-0821, demonstrating hexagonal crystal structure belonging P63/mmc for Mg alloy ( $a=b=3.2094$  Å and  $c=5.211$  Å). This result is also well matched with reported literature<sup>16-19</sup>.

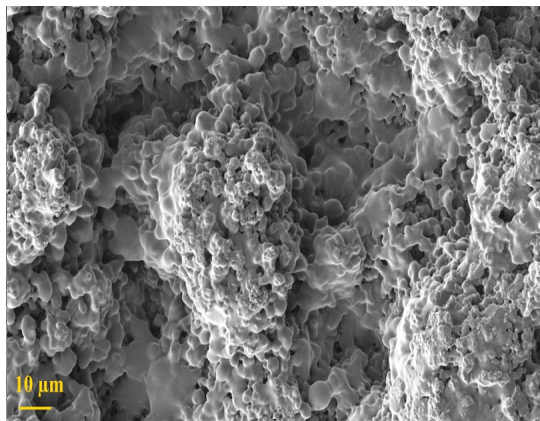
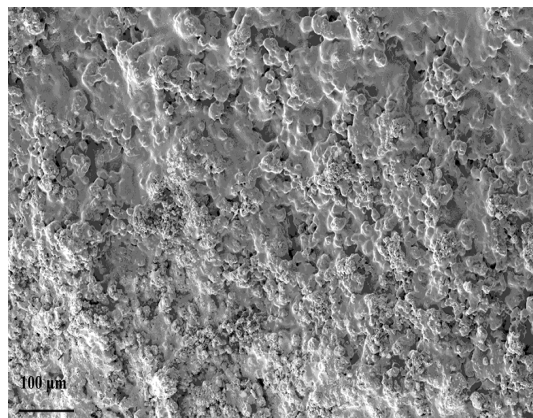
The Sc<sub>2</sub>O<sub>3</sub> coated AZ31 alloy XRD pattern is shown below. The scandium oxide peaks well matched with standard JCPDS file no: 42-1463, showing the cubic crystal structure ( $a=b=c=9.845$  Å) that belongs to Ia3 space group. The peaks at 18.08, 31.4, 36.4, 52.5 and 59.2° corresponds to (211), (222), (400), (440) and (611) planes of cubic Sc<sub>2</sub>O<sub>3</sub>. The base AZ31 alloy peaks demonstrated very low intensity peaks in figure, due to the thick coating of Sc<sub>2</sub>O<sub>3</sub>. This result is also well matched with reported literature<sup>20-22</sup>.

The GeO<sub>2</sub> coated AZ31 alloy XRD pattern is depicted in Fig. 3. Germanium oxide peaks well matched with standard JCPDS file no: 04-0497, showing the hexagonal crystal structure ( $a=b=4.987$  Å,  $c=5.65$  Å) that belongs to P31 space group. The peaks at 20.5°, 25.96°, 38.0°, 41.8° and 66.0° corresponds to (100), (101), (102), (201), (103), (212), (302) and (310) planes of hexagonal GeO<sub>2</sub><sup>23-26</sup>. The base AZ31 alloy peaks demonstrated very low intensity peaks in figure, due to the thick GeO<sub>2</sub>.

Fig. 2. XRD pattern for  $\text{Sc}_2\text{O}_3$  coated AZ31 alloyFig. 3. XRD pattern for  $\text{GeO}_2$  coated AZ31 alloy

### FESEM analysis

The surface morphology of  $\text{Sc}_2\text{O}_3$  and  $\text{GeO}_2$  are presented in Fig. 4 and 5, respectively. Both the scandium oxide and germanium oxide powders show their individual particles with irregular shapes or morphology.

Fig. 4. Surface morphology of  $\text{Sc}_2\text{O}_3$  coated AZ31 alloyFig. 5. Surface morphology of  $\text{GeO}_2$  coated AZ31 alloy

### FTIR analysis

The functional groups of  $\text{Sc}_2\text{O}_3$  and  $\text{GeO}_2$  were analyzed by Fourier Transform Infrared Spectroscopy (FTIR) and presented in Fig. 6 and 7, respectively.

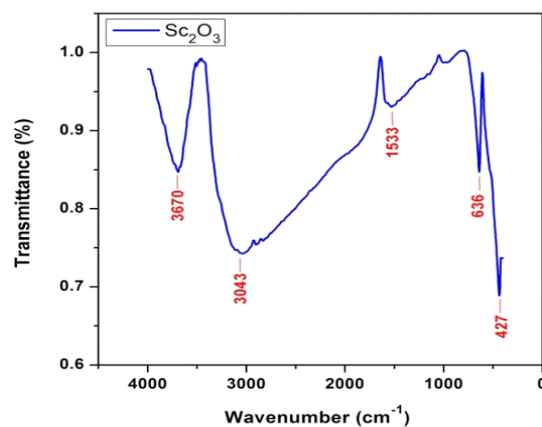
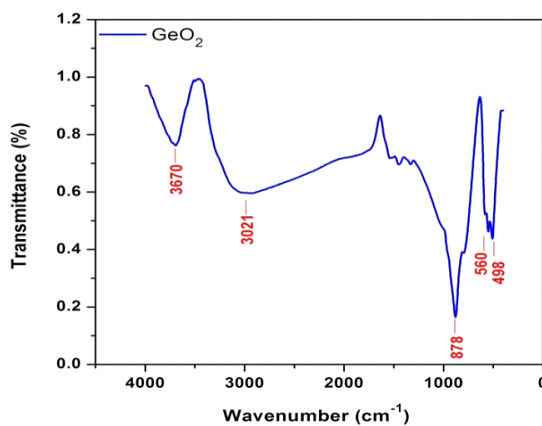
Fig. 6. FTIR spectrum of  $\text{Sc}_2\text{O}_3$  compoundFig. 7. FTIR spectrum of  $\text{GeO}_2$  compound

Figure 6 shows the FTIR spectrum for  $\text{Sc}_2\text{O}_3$  compound, where it is noticed that the peaks

at 427, 636, 1533, 3043 and 3670  $\text{cm}^{-1}$ . The bands at 427 and 636  $\text{cm}^{-1}$  strongly shows the typical characteristic peaks for Sc-O bands in cubic  $\text{Sc}_2\text{O}_3$ . The peaks at 1533  $\text{cm}^{-1}$  might be attributed to the presence of C=O stretching, while the 3040  $\text{cm}^{-1}$  shows the presence of olefinic compounds. The band at 3670  $\text{cm}^{-1}$  shows the hydroxyl stretching<sup>27,28</sup>.

Similarly, Fig. 7 shows the FTIR spectrum of  $\text{GeO}_2$  compound, where it is noticed that the peaks at 498, 560, 878, 3021 and 3670  $\text{cm}^{-1}$ . The peaks at 498, 560  $\text{cm}^{-1}$  corresponds to the  $V_4$  vibration mode in  $\text{GeO}_4$  tetrahedra<sup>29,30</sup>. A strong absorption peak at 878  $\text{cm}^{-1}$  demonstrates the  $V_3$  vibration mode, which is the distorted tetrahedral structure of  $\text{GeO}_2$ . The band at 3021 and 3670  $\text{cm}^{-1}$  are attributed to olefinic and hydroxyl stretching.

### Raman analysis

The Raman spectrum of  $\text{Sc}_2\text{O}_3$  compound is presented in Fig. 8. The Raman modes observed at 194, 320, 538, 420, 495, and 525  $\text{cm}^{-1}$ . The major vibration band at 420  $\text{cm}^{-1}$  can be assigned to totally symmetric Ag and Fg-type modes of octahedra of  $\text{ScO}_6$ <sup>31-33</sup>.

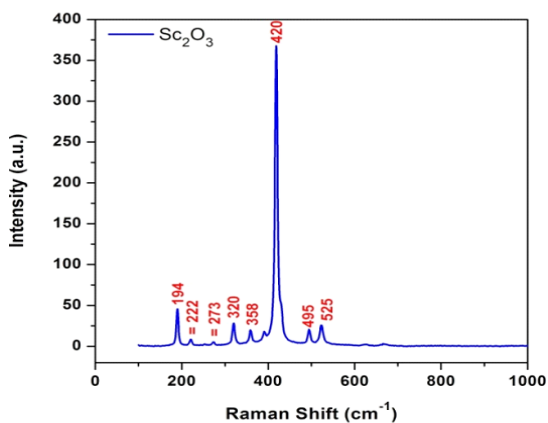


Fig. 8. Raman spectrum of  $\text{Sc}_2\text{O}_3$

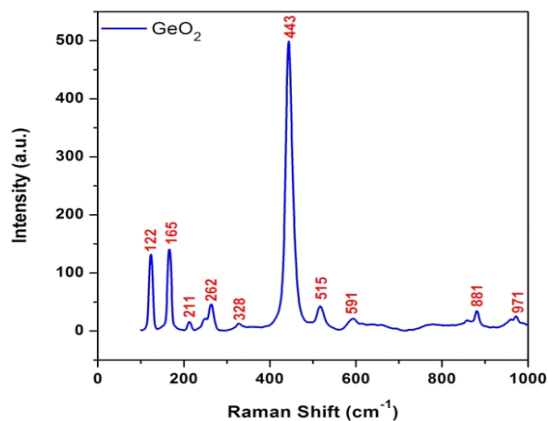


Fig. 9. Raman spectrum of  $\text{GeO}_2$

The spectrum of  $\text{GeO}_2$  is presented in Fig. 9. The Raman modes observed at 122, 165, 211, 262, 328, 443, 515, 591, 881 and 971  $\text{cm}^{-1}$ . The strong peak 443  $\text{cm}^{-1}$  demonstrates the hexagonal  $\text{GeO}_2$  and weak peak at 328  $\text{cm}^{-1}$  shows the  $\text{Ge}^{34, 35}$ . Moreover, the disorder-induced peak (1350  $\text{cm}^{-1}$ ) and graphite peak (1580  $\text{cm}^{-1}$ ), which are caused by C when TaC + C phase is formed. Moreover, the disorder-induced peak (1350  $\text{cm}^{-1}$ ) and graphite peak (1580  $\text{cm}^{-1}$ ), which are caused by C when TaC + C phase is formed. Moreover, the disorder-induced peak (1350  $\text{cm}^{-1}$ ) and graphite peak (1580  $\text{cm}^{-1}$ ), which are caused by C when TaC + C phase is formed. Electrochemical analysis Corrosion behavior of uncoated AZ31,  $\text{Sc}_2\text{O}_3$  and  $\text{GeO}_2$  coatings over AZ31 alloy was studied in 3.5% NaCl medium with an assembly consisting of three electrode system, where Pt as counter electrode, AZ31 alloy samples with and without coatings were as working electrodes and SCE as reference electrode.

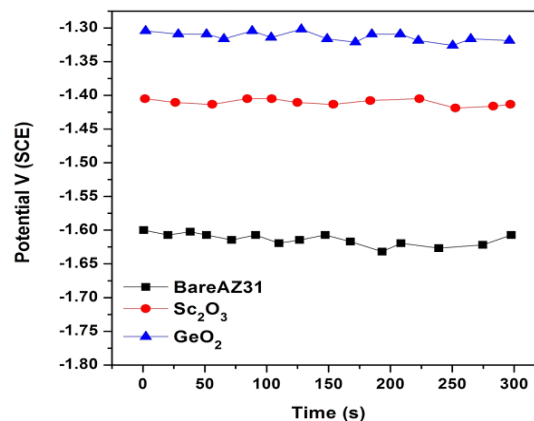


Fig. 10. Open circuit potentials of uncoated AZ31,  $\text{Sc}_2\text{O}_3$  coated and  $\text{GeO}_2$  coated AZ31 alloy

From the figure it is noticed that the corrosion potential or equilibrium potentials of the coated samples, showed a positive shift in the potential or noble shift, which is beneficial for the stability of the alloy. The bare alloy showed -1.7 V (SCE) corrosion potential, while the  $\text{Sc}_2\text{O}_3$  coated AZ31 alloy showed -1.4 V (SCE) and  $\text{GeO}_2$  coated AZ31 alloy showed -1.3 V (SCE). The  $\text{GeO}_2$  coated AZ31 alloy demonstrated more noble shift.

The linear polarization studies of uncoated AZ31 and  $\text{Sc}_2\text{O}_3$  coated and  $\text{GeO}_2$  coated AZ31 alloys are shown in Fig. 11. From the figure, it is noticed that bare AZ31 demonstrated higher corrosion susceptibility than coated samples. The

corrosion rate details are as follows, the bare alloys exhibited the  $i_{\text{corr}}$  of  $3.4 \times 10^{-4}$  mA/cm<sup>2</sup>, Sc<sub>2</sub>O<sub>3</sub> coated AZ31 alloy exhibited  $i_{\text{corr}}$  of  $5.4 \times 10^{-9}$  mA/cm<sup>2</sup> and GeO<sub>2</sub> coated AZ31 alloy exhibited  $i_{\text{corr}}$  of  $2.59 \times 10^{-9}$  mA/cm<sup>2</sup>. The results shows that GeO<sub>2</sub> coated AZ31 alloy demonstrated better performance. The electrochemical impedance curves of bare AZ31 and Sc<sub>2</sub>O<sub>3</sub> coated and GeO<sub>2</sub> coated AZ31 alloys in NaCl (3.5%) electrolyte is shown Fig. 12. The EIS studies were studied in the frequency range of 1MHz to 100 mHz at open circuit potential.

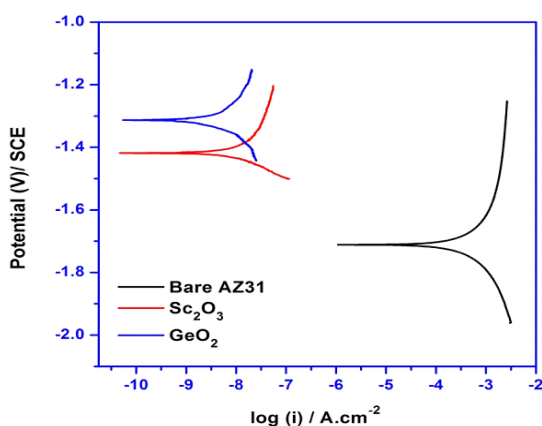


Fig. 11. Linear polarization studies of uncoated AZ31 and Sc<sub>2</sub>O<sub>3</sub> coated and GeO<sub>2</sub> coated AZ31 alloy

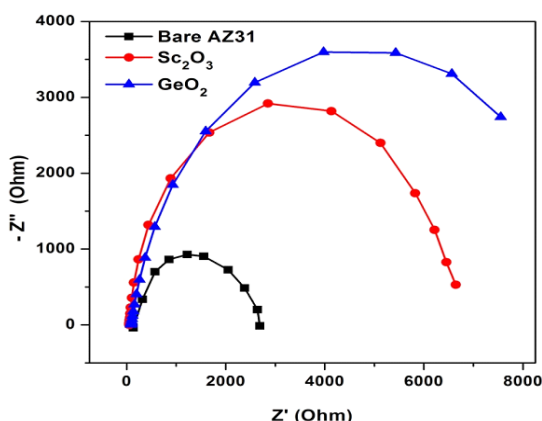


Fig. 12. EIS curves of AZ31 and Sc<sub>2</sub>O<sub>3</sub> and GeO<sub>2</sub> coated AZ31 alloys

Table 1: Electrochemical polarization data of AZ31 and Sc<sub>2</sub>O<sub>3</sub> and GeO<sub>2</sub> coated AZ31 alloys

S.No	Electrode	$E_{\text{corr}}$ (V vs SCE)	$i_{\text{corr}}$ (mA/cm <sup>2</sup> )
01	Bare AZ31 alloy	-1.7	$3.4 \times 10^{-4}$
02	Sc <sub>2</sub> O <sub>3</sub> coated AZ31 alloy	-1.4	$5.4 \times 10^{-9}$
03	GeO <sub>2</sub> coated AZ31 alloys	-1.3	$2.59 \times 10^{-9}$

The EIS studies shows that bare AZ31 alloy showed very less corrosion resistance, while the Sc<sub>2</sub>O<sub>3</sub> coated AZ31 alloy showed intermediate performance and GeO<sub>2</sub> coated AZ31 alloy showed superior corrosion resistance.

White *et al.*, fabricated TiO<sub>2</sub> coating over AZ31 alloy using plasma electrolytic oxidation (PEO), where the coating demonstrated enhanced corrosion protection to Mg alloy<sup>36</sup>. The coating showed the noble shift in corrosion potential up to -1.4 V (SCE) in 3.5% NaCl electrolyte. Similarly, Chen *et al.*, developed MgO, MgAl<sub>2</sub>O<sub>4</sub> and MgSiO<sub>3</sub> composed coating through micro arc oxidation process and demonstrated that the ceramic coated sample showed corrosion potential of ~1.5 V in 3.5% NaCl medium<sup>37</sup>. Tan *et al.*, developed Ca-P coatings on AZ31 Mg alloy via chemical deposition and noticed that Ca-P coating dramatically decreased the corrosion rates and improved corrosion resistance. The authors demonstrated the corrosion potential up to -1.5 V (SCE) in 3.5% NaCl medium<sup>38</sup>. In this work, the GeO<sub>2</sub> coated AZ31 alloy showed the corrosion potential of ~ -1.3 V (SCE) and corrosion current density of  $2.59 \times 10^{-9}$  mA/cm<sup>2</sup> in 3.5% NaCl medium. This work demonstrated enhanced corrosion protection for AZ31 alloy with proposed coatings in comparison with literature and paves new pathway for the corrosion protection improvement of magnesium alloys.

## CONCLUSION

- The GeO<sub>2</sub> (germanium dioxide) and Sc<sub>2</sub>O<sub>3</sub> (scandium trioxide) were developed as coatings on AZ31 alloy using polymer binder.
- The corrosion studies were analyzed using a three electrode system in 3.5% NaCl electrolyte. The bare AZ31 alloy showed open circuit potential ( $E_{\text{corr}}$ ) of -1.7 V (SCE) and  $i_{\text{corr}}$  of  $3.4 \times 10^{-4}$  mA/cm<sup>2</sup>, while the Sc<sub>2</sub>O<sub>3</sub> coated AZ31 alloy exhibited  $E_{\text{corr}}$  of -1.4 V (SCE) and  $i_{\text{corr}}$  of  $5.4 \times 10^{-9}$  mA/cm<sup>2</sup> and while the GeO<sub>2</sub> coated AZ31 alloy exhibited  $E_{\text{corr}}$  of -1.3 V (SCE) and  $i_{\text{corr}}$  of  $2.59 \times 10^{-9}$  mA/cm<sup>2</sup>.
- The results reveal that the GeO<sub>2</sub> coated AZ31 alloy demonstrated higher corrosion resistance than of bare and Sc<sub>2</sub>O<sub>3</sub> coated AZ31 alloy.

**ACKNOWLEDGEMENT**

The authors would like to thank Department of Industrial Chemistry, Alagappa University, Karaikudi, India and the Post graduate & Research Department of Chemistry, Raja Doraisingam

Government Arts College, Sivaganga, for providing the academic support and research support.

**Conflict of Interest**

The authors declare that the current work has not conflict interest.

**REFERENCE**

1. Wu, R.Z.; Yan, Y.D.; Wang, G.X.; Murr L.E.; Han W.; Zhang, Z.W.; Zhang M.L. *Int. Mater. Rev.*, **2015**, *60*, 65–100.
2. Thomas, S.; Medhekar, N.V.; Frankel, G.S.; Birbilis, N. *Curr. Opin. Solid State Mater. Sci.*, **2015**, *19*, 85–94.
3. Hou, L.; Wang, T.; Wu, R.; Zhang, J.; Zhang, M.; Dong, A.; Sun, B.; Betsofen, S.; Krit B. J. *Mater. Sci. Technol.*, **2018**, *34*, 317–323.
4. Mordike, B.L.; Ebert, T. *Mater. Sci. Eng.*, **2001**, *302*, 37–45.
5. Shahabi-Navid M.; Esmaily, M.; Svensson, J.E.; Halvarsson, M.; Nyborg, L.; Cao, Y.; Johansson, L.G. *J. Electrochem. Soc.*, **2014**, *61*, C277–C287.
6. M. Esmaily, D.B. Blücher, R.W. Lindstrom, J.E. Svensson, L.G. Johansson, J. *Journal of The Electrochemical Society.*, **2015**, *162*(6), 260–269.
7. Electrochem. Soc. 2015, 162, C260–C269
8. Danaie, M.; Asmussen, R.M.; Jakupi, P.; Shoesmith, D.W.; Bottona G.A. *Corros. Sci.*, **2013**, *77*, 151–163.
9. Pu, Z.; Yang, S.; Song, G.-L.; Dillon Jr. O.W.; Puleo, D.A.; Jawahir, I.S. *Scr. Mater.*, **2011**, *65*, 520–523.
10. Esmaily, M.; Shahabi-Navid, M.; Svensson, J.E.; Halvarsson, M.; Nyborg, L.; Cao, Y.; Johansson, L.G. *Corros. Sci.*, **2015**, *90*, 420–433.
11. Ha, H.; Kim, H.; Baek, S.; Kim, B.; Sohn, S.; Shin, H.; Jeong, H.Y.; Park, S.H.; Yim, C.D.; You, B.S.; Lee, J.G.; Park, S.S. *Scr. Mater.*, **2015**, *109*, 38–43.
12. Singh Raman, R.K.; Birbilis, N.; Efthimiadis, J. *Corros. Eng. Sci. Technol.*, **2004**, *39*, 346–350.
13. Asmussen, R.M.; Jakupi, P.; Danaie, M.; Bottonb, G.A.; Shoesmith D.W. *Corros. Sci.*, **2013**, *75*, 114–122.
14. Wu, G.; Dai, W.; Zheng, H.; Wang, A. *Surf. Coat. Technol.*, **2010**, *205*, 2067–073.
15. Han, B. *Int. J. Electrochem. Sci.*, **2017**, 9829–9843.
16. Yaowei, Y.; Wei, F.; Xiang, Z.; Qilin, D.; Jianguo, Y. *Rare Metal Mat Eng.*, **2017**, *46*, 3176–3181.
17. Sunil, B. R.; Ganesh, K. V.; Pavan, P.; Vadapalli, G.; Swarnalatha, C.; Swapna, P.; Bindukumar, P.; Pradeep Kumar Reddy, G. (2016). *J. Magnes. Alloy.*, **2016**, *4*, 15–21.
18. Fridrich, H.E.; Mordike, B.L. *Magnesium Technology, Springer, Germany.*, **2006**.
19. Mordike, B. L.; Ebert, T. *Mater. Sci. Eng. A.*, **2001**, *302*, 37–45.
20. Avedesian, M.M.; Baker, H. ASM Specialty Handbook, Magnesium and Magnesium Alloys, *ASM International, USA.*, **1999**.
21. Krsmanovic, R.; Lebedev, O. I.; Speghini, A.; Bettinelli, M.; Polizzi, S.; Tendeloo, G. V. *Nanotechnology.*, **2006**, *17*, 2805–2812.
22. Liu, D.; Lei, W.; Li, Y.; Ma, Y.; Hao, J.; Chen, X.; Jin, Y.; Liu, D.; Yu, S.; Cui, Q.; Zou, G. *Inorganic Chemistry.*, **2009**, *48*, 8251–8256.
23. Chen, C. P.; Hong, M.; Kwo, J.; Cheng, H. M.; Huang, Y. L.; Lin, S. Y.; Chi, J.; Lee, H.Y.; Hsiesh, Y.F.; Mannaerts, J. P. *J. Cryst. Growth.*, **2005**, *278*, 638–642.
24. Zhao, J.; Yang, L.; McLeod, J.; Liu, L. *Sci Rep.*, **2015**, *5*, 17779.
25. Xie, M.; Nishimura, T.; Yajima, T.; Toriumi, A. *J. Appl. Phys.*, **2020**, *127*, 024101.
26. Wang, S. K.; Kita, K.; Nishimura, T.; Nagashio, K.; Toriumi, A. “Interfacial reaction induced GeO desorption, GeO<sub>2</sub> crystallization and non-uniform void formation in GeO<sub>2</sub>/Ge stack,” in Materials Research Society (MRS) Spring Meeting (MRS, San Francisco, USA, **2011**), 7.7.

27. Wang, S. K.; Kita, K.; Nishimura, T.; Nagashio, K.; Toriumi, A. *J. Appl. Phys.*, **2011**, *50*, 10PE04.
28. Feijoo, P.C.; del Prado, A.; Toledano-Luque, M.; San Andrés, E.; Lucía, M.L. *J. Appl. Phys.*, **2010**, *107*, 084505.
29. Li, J.-G.; Ikegami, T.; Mori T. *J. Am. Ceram. Soc.*, **2005**, *88*, 817–821
30. Ngo, D. T.; Kalubarme, R. S.; Le, H. T. T.; Park, C.-N.; Park, C. *J. Nanoscale.*, **2015**, *7*, 2552–2560.
31. Wu, H. P.; Liu, J. F.; Ge, M. Y.; Niu, L.; Zeng, Y. W.; Wang, Y. W.; Jiang, J. Z. *Chem. Mater.*, **2006**, *18*, 1817–1820.
32. Kaminskii, A. A.; Bagaev, S. N.; Ueda, K.; Takaichi, K.; Lu, J.; Shirakawa, A.; Rhee, H. *Laser Phys. Lett.*, **2005**, *2*, 30–35.
33. Repelin, Y.; Proust, C.; Husson, E.; Beny, J. *M. J. Solid State Chem.*, **1995**, *118*, 163.
34. Kaminskii, A. A.; Bagaev, S. N.; Ueda, K.; Takaichi, K.; Lu, J.; Shirakawa, A.; Yagi, H.; Yanagitani, T.; Eichler, H. J.; Rhee, H. *Laser Phys. Lett.*, **2005**, *2*, 30.
35. Atuchin, V. V.; Gavrilova, T. A.; Gromilov, S. A.; Kostrovsky, V. G.; Pokrovsky, L. D.; Troitskaia, I. B.; Vemuri, R. S.; Carbajal-Franco, G.; Ramana, C. V. *Cryst. Growth Des.*, **2009**, *9*, 1829.
36. Shinde, S. L.; Nanda, K. K. *Cryst Eng Comm.*, **2013**, *15*, 4049.
37. White, L.; Koo, Y.; Yun, Y.; Sankar J. *J. Nanomater.*, **2013**, 1–8.
38. Chen, F.; Zhou, H.; Yao, B.; Qin, Z.; Zhang, Q. *Surf. Coat. Technol.*, **2007**, *201*, 4905–4908.
39. Tan, L.; Wang, Q.; Geng, F.; Xi, X.; Qiu, J.; Yang, K. T. *Nonferr Metal Soc.*, **2010**, *20*, s648–s654.